

Overview on All Reactions Linked to GPDs

Marc Vanderhaeghen ^a

^aInstitut für Kernphysik, Johannes Gutenberg-Universität, D-55099 Mainz, Germany

A short overview is given on how generalized parton distributions (GPDs) enter in a variety of hard exclusive processes such as deeply virtual Compton scattering (DVCS) and hard meson electroproduction reactions on the nucleon. We firstly discuss the links between GPDs and elastic nucleon form factors which represent powerful constraints on parametrizations of GPDs. Subsequently, we show some key observables which are sensitive to the various hadron structure aspects of the GPDs, and which are at present under experimental investigation at different facilities (HERMES, H1/ZEUS, JLab and Compass), or will be addressed by experiments in the near future.

1. Introduction

Generalized parton distributions (GPDs), are universal non-perturbative objects entering the description of hard exclusive electroproduction processes (see Refs. [1–3] for reviews and references). In leading twist there are four GPDs for the nucleon, i.e. H , E , \tilde{H} and \tilde{E} , which are defined for each quark flavor (u , d , s). These GPDs depend upon the different longitudinal momentum fractions $x + \xi$ ($x - \xi$) of the initial (final) quark and upon the overall momentum transfer $t = \Delta^2$ to the nucleon (see Fig. 1). As the

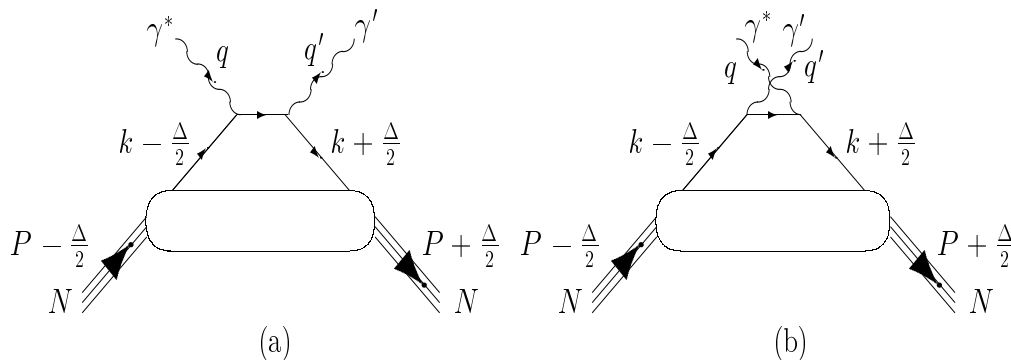


Figure 1. “Handbag” diagrams for the DVCS process, containing the GPDs.

momentum fractions of initial and final quarks are different, one accesses quark momentum correlations in the nucleon. Furthermore, if one of the quark momentum fractions is negative, it represents an antiquark and consequently one may investigate $q\bar{q}$ configurations in the nucleon. Therefore, these functions contain a wealth of new nucleon structure information, generalizing the information obtained in inclusive deep inelastic scattering.

To access this information, a general parametrization for all four GPDs has been given in [3]. For the GPDs H and E , a two-component parametrization has been developed consisting of a double distribution [4,5] and a D-term [6] part. The latter is sensitive to scalar-isoscalar $q\bar{q}$ configurations in the nucleon. The parameters entering this parametrization can be related in a rather general way to such (not yet measured) quantities as the contribution of the nucleon spin carried by the quark total angular momentum (J^u, J^d , etc.), $\bar{q}q$ components of the nucleon wave function (in particular the D-term and the “vector meson” part of the GPD E), the strength of the skewedness effects in the GPDs (encoded in their ξ -dependence), the quark structure of $N \rightarrow N^*, \Delta$ transitions, the weak electricity GPD in nucleon to hyperon transitions, flavor $SU(3)$ breaking effects, and others. Furthermore, it has been shown that by a Fourier transform of the t -dependence of GPDs, it is conceivable to access the distributions of parton in the transverse plane, see Refs. [7,8].

In this short paper, only a very limited selection of the above topics can be touched upon, and the reader is referred to the other contributions in these proceedings for more discussions on the above subjects.

2. Nucleon electromagnetic form factors

We start by discussing the t -dependence of the GPDs which is directly related to nucleon elastic form factors through sum rules. In particular, the nucleon Dirac and Pauli form factors $F_1(t)$ and $F_2(t)$ can be calculated from the GPDs H and E through the following sum rules for each quark flavor ($q = u, d$)

$$F_1^q(t) = \int_{-1}^{+1} dx H^q(x, \xi, t), \quad F_2^q(t) = \int_{-1}^{+1} dx E^q(x, \xi, t). \quad (1)$$

We can choose $\xi = 0$ in the previous equations, and model $H(x, 0, t)$ and $E(x, 0, t)$ subsequently. For the GPD $H(x, 0, t)$, a plausible ansatz at low $-t$ is a Regge form as discussed in [3]. This leads to the following integrals to calculate the Dirac form factors for u - and d -quark flavors :

$$F_1^u(t) = \int_0^{+1} dx u_v(x) \frac{1}{x^{\alpha_1' t}}, \quad F_1^d(t) = \int_0^{+1} dx d_v(x) \frac{1}{x^{\alpha_1' t}}, \quad (2)$$

where $u_v(x)$ and $d_v(x)$ are the u - and d -quark valence distributions, and where α_1' is the slope of the leading Regge trajectory. The proton and neutron Dirac form factors then follow from

$$F_1^p(t) = e_u F_1^u(t) + e_d F_1^d(t), \quad F_1^n(t) = e_u F_1^d(t) + e_d F_1^u(t), \quad (3)$$

where by construction $F_1^p(0) = 1$, and $F_1^n(0) = 0$.

Using the above ansatz, the Dirac mean squared radii of proton and neutron can be calculated as :

$$r_{1,p}^2 = -6 \alpha_1' \int_0^{+1} dx \left\{ e_u u_v(x) + e_d d_v(x) \right\} \ln x, \quad (4)$$

$$r_{1,n}^2 = -6 \alpha_1' \int_0^{+1} dx \left\{ e_u d_v(x) + e_d u_v(x) \right\} \ln x, \quad (5)$$

which yields for the electric mean squared radii of proton and neutron :

$$r_{E,p}^2 = r_{1,p}^2 + \frac{3}{2} \frac{\kappa_p}{m_N^2}, \quad r_{E,n}^2 = r_{1,n}^2 + \frac{3}{2} \frac{\kappa_n}{m_N^2}, \quad (6)$$

where κ_p (κ_n) are the proton (neutron) anomalous magnetic moments.

In Fig. 2, we show the proton and neutron rms radii as function of the Regge slope α'_1 , which is the only free parameter in the ansatz of Eq. (2). One notes that the neutron rms radius is dominated by the Foldy term (term proportional to κ_n in Eq. (6)), which gives $r_{E,n}^2 = -0.126 \text{ fm}^2$. Therefore, a relatively wide range of values α'_1 are compatible with the neutron data. However for the proton, a rather narrow range of values around $\alpha'_1 = 1.0 - 1.1 \text{ GeV}^{-2}$ are favored. Such value is close to the expectation from Regge slopes for meson trajectories, therefore supporting the ansatz of Eq. (2).

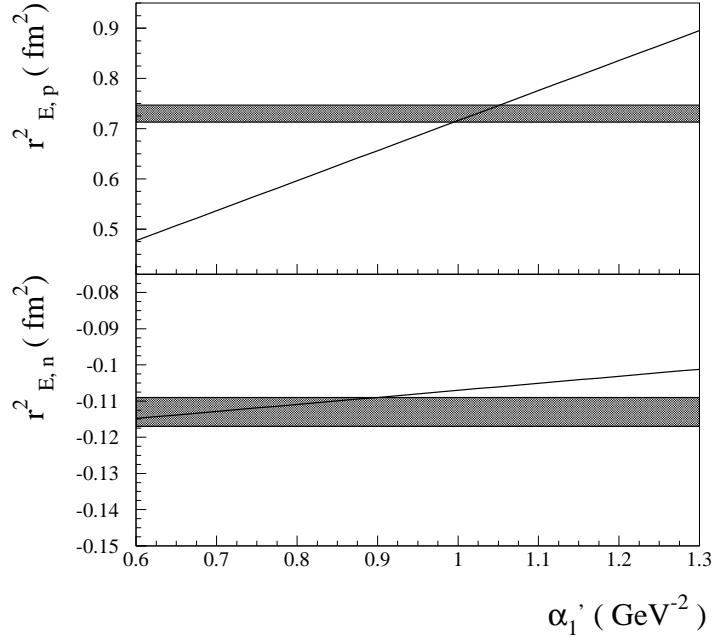


Figure 2. Proton and neutron electric mean squared radii $r_{E,p}^2$ (upper panel) and $r_{E,n}^2$ (lower panel), Eq. (6). The calculations show the dependence of the Regge ansatz according to Eqs. (4,5) on the Regge slope α'_1 . For the quark distributions, the MRST01 NNLO parametrization [9] at scale $\mu^2 = 1 \text{ GeV}^2$ was used in the calculations. The shaded bands correspond to the experimental values.

To calculate the electric and magnetic form factors of the nucleon, one also needs to calculate the Pauli form factor F_2 , besides F_1 . For F_2 , we use an ansatz which is based on a valence quark distribution for the valence part of $E(x, 0, t)$ entering in Eq. (1). This leads to the following integrals for the proton and neutron Pauli form factors :

$$F_2^u(t) = \int_0^{+1} dx \kappa_u \frac{1}{2} u_v(x) \frac{1}{x^{\alpha_2' t}}, \quad F_2^d(t) = \int_0^{+1} dx \kappa_d d_v(x) \frac{1}{x^{\alpha_2' t}}, \quad (7)$$

where κ_u and κ_d are given by $\kappa_u = 2\kappa_p + \kappa_n$, and $\kappa_d = \kappa_p + 2\kappa_n$.

In Fig. 3, we show the predictions of the above discussed Regge ansatz for the proton

and neutron form factors. For both proton and neutron magnetic form factors, one sees that the Regge forms reproduce the experimentally observed dipole behavior up to about $-t = 0.5 \text{ GeV}^2$. Such behavior follows in the present ansatz from the behavior of valence quark distributions at small/intermediate values of x . At larger values of $-t$, the Regge form expectedly falls short of the data as one expects a transition to the perturbative behavior ($\sim 1/t^2$) of the magnetic form factors. For the ratio of electric to magnetic proton form factors, one interestingly sees that the Regge form leads to a decreasing ratio with $-t$. Although the simple Regge model falls too fast with $-t$, the decreasing trend is in qualitative agreement with the data at larger $-t$ from JLab [10,11]. For the neutron magnetic form factors, one obtains a remarkable good description up to $-t \simeq 1 \text{ GeV}^2$.

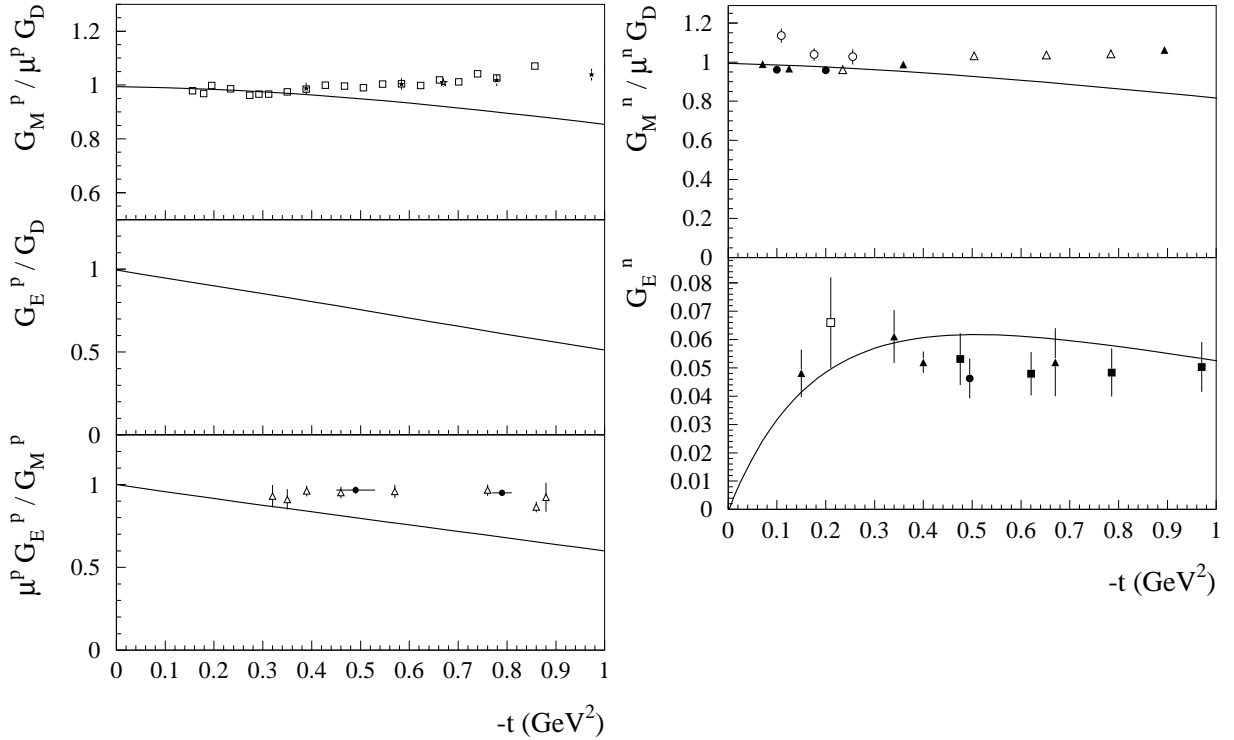


Figure 3. Left side : proton magnetic (upper panel) and electric (middle panel) form factors compared to the dipole form $G_D(t) = 1/(1 - t/0.71)^2$, as well as the ratio of both form factors (lower panel). Right side : neutron magnetic (upper panel) and electric (lower panel) form factors. The curves correspond to the Regge ansatz of Eqs.(2) and (7) , with $\alpha'_1 = 1.1 \text{ GeV}^{-2}$, $\alpha'_2 = 1.1 \text{ GeV}^{-2}$. The references to the data can be found in [12].

The simple Regge ansatz discussed here [12], catches the basic features of the nucleon electromagnetic form factors at $-t < 0.5 \text{ GeV}^2$. For $-t > 1 \text{ GeV}^2$, an overlap representation linking the nucleon Dirac form factor to GPDs has been given in Refs. [13,14], describing the trend of the data. A topic for further study is to incorporate both small- t and large- t regimes in a unified parametrization. This is needed to perform the Fourier transform for the t -dependence of GPDs in order to map out the distribution of partons in the transverse plane.

3. DVCS beam-helicity asymmetry

We next turn to the DVCS observables and their dependence on the GPDs. At intermediate lepton beam energies, one can extract the imaginary part of the DVCS amplitude through the $\vec{e}p \rightarrow ep\gamma$ reaction with a polarized lepton beam, by measuring the out-of-plane angular dependence (in the angle ϕ) of the produced photon [15]. It was found in Refs. [16,17] that the resulting electron single spin asymmetry (SSA)

$$\mathcal{A}^{\text{SSA}} = \frac{\sigma_{e,h=+1/2} - \sigma_{e,h=-1/2}}{\sigma_{e,h=+1/2} + \sigma_{e,h=-1/2}}, \quad (8)$$

with $\sigma_{e,h}$ the cross section for an electron of helicity h , can be sizeable for HERMES ($E_e = 27$ GeV) and JLab ($E_e = 4 - 11$ GeV) beam energies. The SSA for the $\vec{e}p \rightarrow ep\gamma$ reaction has recently been measured in pioneering experiments at HERMES [18] and JLab/CLAS [19], which are shown in Fig. 4. These experiments display already at the accessible values of $Q^2 \simeq 1 - 2.5$ GeV² predominantly a $\sin\phi$ dependence, indicating a dominance of the twist-2 DVCS amplitude. Furthermore, the observed magnitude is in good agreement with the theoretical calculations of Refs. [20,21] in terms of GPDs. These first experiments give strong indication that the SSA is a promising observable to get access to GPDs. Once the leading order mechanism in terms of GPDs is confirmed by experiment, the measured helicity difference in Eq. (8) is directly proportional to the GPDs along the line $x = \xi$, and one may proceed to map out the 'envelope' function $H(\xi, \xi, t)$, and analogously for E , \tilde{H} and \tilde{E} .

Dedicated experiments to measure the SSA with improved accuracy in a large kinematic range are already planned and underway both at JLab [22,23] and HERMES [24,25].

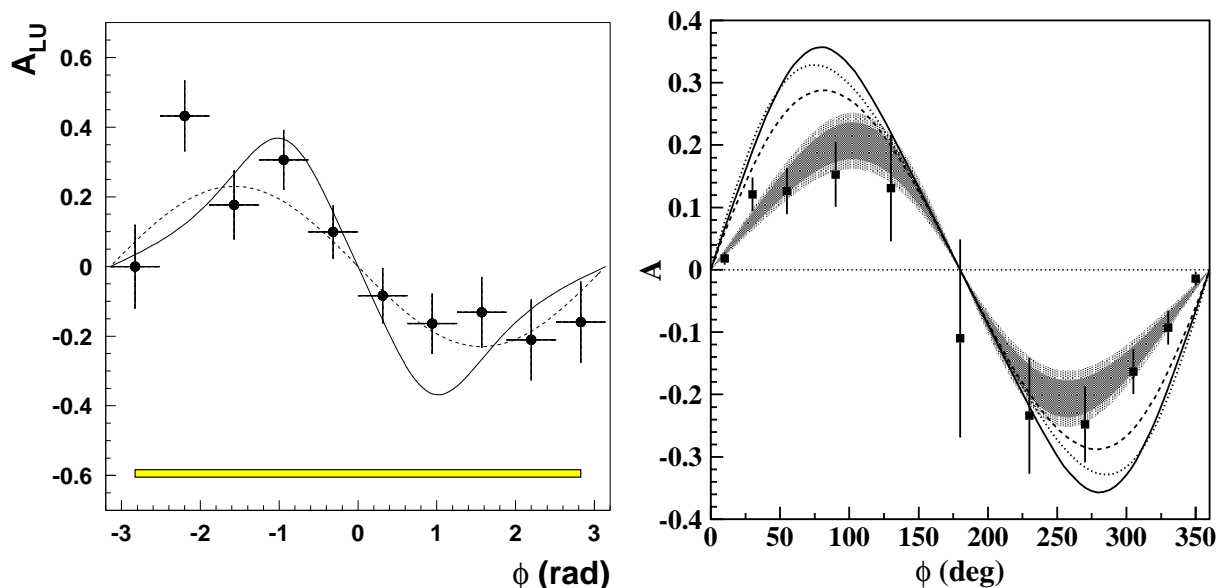


Figure 4. The DVCS beam helicity asymmetry as measured at HERMES [18] (left panel) and JLab/CLAS [19] (right panel). Full curves are the twist-2 + twist-3 predictions of Ref. [20].

4. DVCS beam-charge asymmetry

Besides the beam-helicity asymmetry for the $\vec{e}p \rightarrow ep\gamma$ reaction, which accesses the imaginary part of the DVCS amplitude, one gets access to the real part of the DVCS amplitude by measuring both $e^+p \rightarrow e^+p\gamma$ and $e^-p \rightarrow e^-p\gamma$ processes. In those reactions, besides the mechanism where the photon originates from a quark (handbag diagrams of Fig. 1, the photon can also be emitted by the lepton lines, in the so-called Bethe-Heitler (BH) process. Because the BH amplitude contains two lepton electromagnetic couplings in contrast to the DVCS process, the interference between BH and DVCS processes changes sign when comparing the $e^+p \rightarrow e^+p\gamma$ and $e^-p \rightarrow e^-p\gamma$ reactions. Therefore, in the difference of cross sections $\sigma_{e^+} - \sigma_{e^-}$, the BH drops out, and one measures the real part of the BH-DVCS interference [26]

$$\sigma_{e^+} - \sigma_{e^-} \sim \Re \left[T^{BH} T^{DVCS*} \right], \quad (9)$$

which is proportional to the *real* (principle value integral) part of the DVCS amplitude. In this way, the difference $\sigma_{e^+} - \sigma_{e^-}$ is sensitive to the GPDs away from the line $x = \xi$.

It has been shown in [20] that this beam-charge asymmetry gets a sizeable contribution from the D-term. The latter encodes $q\bar{q}$ scalar-isoscalar correlations in the nucleon as shown in Fig. 5 (left side), and has been estimated in the chiral quark soliton model [27].

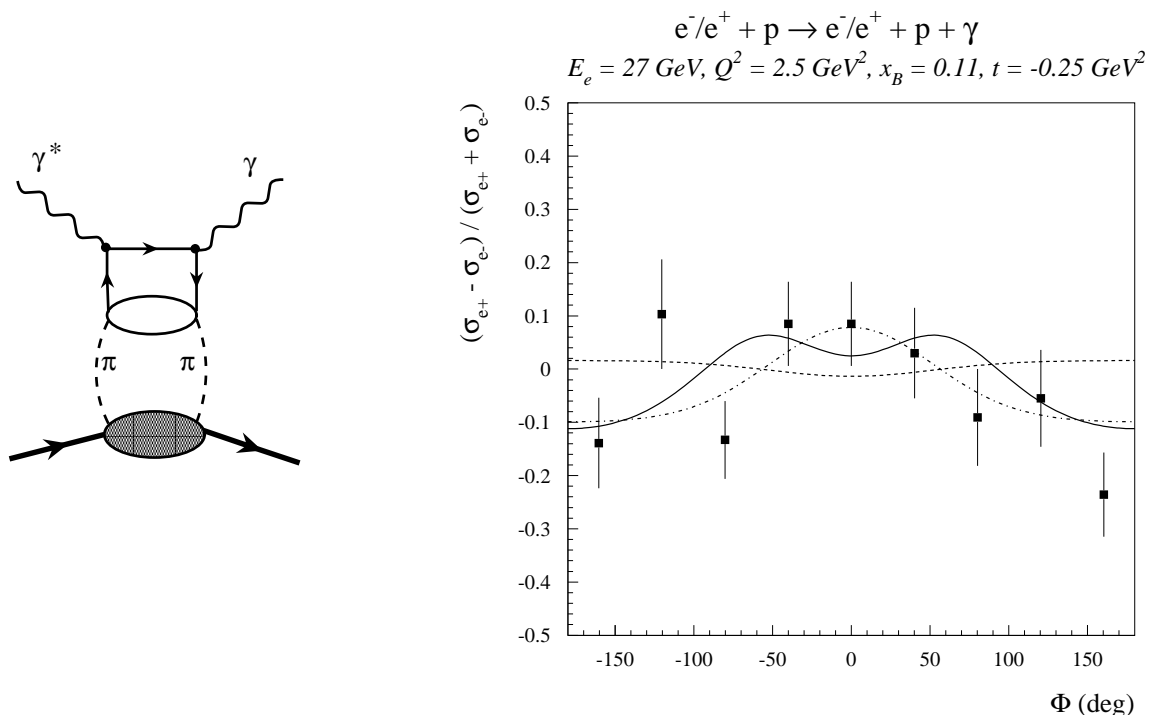


Figure 5. Left side : Model contribution to the D-term entering the GPDs H and E . Right side : the DVCS beam-charge asymmetry. The preliminary data are from HERMES [28]. Theoretical predictions are from Ref. [20] : the calculations of the twist-2 DVCS amplitude with (without) D-term are shown by the dashed-dotted (dashed) curves. The full curve is obtained when adding twist-3 effects in addition to the D-term.

The beam-charge asymmetry associated with DVCS has been accessed experimentally very recently at HERMES, as reported in this Workshop [28]. The preliminary data are shown in Fig. 5, together with the theoretical predictions. The experimental asymmetry shows a $\cos\phi$ dependence with magnitude $\sim 0.10-0.15$, and favors the calculations which include the D-term. This opens up the perspective to study (mesonic) $q\bar{q}$ components in the nucleon wavefunction in a systematic and model independent way. Further measurements of the beam-charge asymmetry associated with DVCS with improved statistics are planned at HERMES [25].

5. Hard meson electroproduction (HMP)

The GPDs reflect the structure of the nucleon independently of the reaction which probes the nucleon. In this sense, they are universal quantities and can also be accessed, in different flavor combinations, through the hard exclusive electroproduction of mesons - $\pi^{0,\pm}, \eta, \dots, \rho^{0,\pm}, \omega, \phi, \dots$ - for which a QCD factorization proof was given in Ref. [29]. This factorization theorem applies when the virtual photon is longitudinally polarized, which corresponds to a small size configuration compared to a transversely polarized photon.

In the following, we consider the vector meson electroproduction processes $\gamma_L^* + N \rightarrow V_L + N$ at large Q^2 on the nucleon N , where V_L ($\rho_L^0, \rho_L^+, \omega_L, \dots$) denotes the produced vector meson with longitudinal polarization. For $\rho_L^0 p$ electroproduction on the proton, the leading order amplitudes involving no spin-flip of the nucleon (A) or involving a nucleon spin-flip (B) are proportional to the following combinations of GPDs [30,16] :

$$A_{\rho_L^0 p} = \int_{-1}^1 dx \frac{1}{\sqrt{2}} (e_u H^u - e_d H^d) \left\{ \frac{1}{x - \xi + i\epsilon} + \frac{1}{x + \xi - i\epsilon} \right\}, \quad (10)$$

$$B_{\rho_L^0 p} = \int_{-1}^1 dx \frac{1}{\sqrt{2}} (e_u E^u - e_d E^d) \left\{ \frac{1}{x - \xi + i\epsilon} + \frac{1}{x + \xi - i\epsilon} \right\}, \quad (11)$$

where $e_u = +2/3$ ($e_d = -1/3$) are the u (d) quark charges respectively.

Recently, ρ_L^0 data have been obtained at HERMES for Q^2 up to 5 GeV², around c.m. energy $W \approx 5$ GeV [31]. The calculations for ρ_L^0 , including a model estimate for power corrections [32], point towards the dominance of the quark exchange mechanism in this intermediate W range. However due to the large size of the power corrections at accessible values of Q^2 , it would be too premature at the present stage to try to extract quark GPDs from these vector meson electroproduction cross sections. To reach this goal, one first needs to get a better theoretical control over the power (higher-twist) corrections, which is an important topic for future work.

Besides the cross section σ_L , the second leading order observable for HMP, is the transverse spin asymmetry, $\mathcal{A}_{V_L N}$ (TSA) for a proton target polarized perpendicular to the reaction plane. For the electroproduction of longitudinally polarized vector mesons, induced by a longitudinal virtual photon, the TSA is given by [3] :

$$\mathcal{A}_{V_L N} = -\frac{2|\Delta_\perp|}{\pi} \frac{\text{Im}(AB^*)/m_N}{|A|^2(1-\xi^2) - |B|^2(\xi^2 + t/(4m_N^2)) - \text{Re}(AB^*)2\xi^2}, \quad (12)$$

which is proportional to the modulus $|\Delta_\perp|$ of the perpendicular component of the momentum transfer Δ , and with A and B given by Eqs. (10-11) in the case of ρ_L^0 . One sees that

the TSA is proportional to the imaginary part of the *interference* of the amplitudes A and B , which contain the GPDs H and E respectively. Therefore, it depends *linearly* on the GPD E . Note that in contrast, both in the DVCS cross sections and SSA as well as in the cross sections for (longitudinally polarized) vector mesons, the GPD E only enters besides a large contribution of the GPD H . Therefore, the transverse spin asymmetry of Eq. (12) provides a unique observable to extract the GPD E .

Besides, one may expect that the theoretical uncertainties and open questions for the meson electroproduction cross sections largely disappear for the TSA, suggesting that it is less sensitive to pre-asymptotic effects and that the leading order expression of Eq. (12) is already accurate at accessible values of Q^2 (in the range of a few GeV^2). Due to its linear dependence on the GPD E , the TSA for longitudinally polarized vector mesons opens up the perspective to extract the total angular momentum contributions J^u and J^d of the u - and d -quarks to the proton spin. In the parametrization for the GPDs E^q presented in Ref. [3], J^u and J^d , enter as free parameters. Due to the different u - and d -quark content of the vector mesons, the asymmetries for the ρ_L^0 , ω_L and ρ_L^+ channels are sensitive to different combinations of J^u and J^d , with ρ_L^0 production mainly sensitive to the combination $2J^u + J^d$, ω_L to the combination $2J^u - J^d$, and ρ_L^+ to the isovector combination $J^u - J^d$.

In Fig. 6, the sensitivity of the TSA for ρ_L^0 production on different values of J^u is shown. The TSA for ρ_L^0 electroproduction displays a pronounced sensitivity to J^u around $x_B \approx 0.4$, where asymmetries are predicted in the -15 % to -30 % range according to the value of J^u . It will therefore be very interesting to provide a first measurement of this asymmetry in the near future, for a transversely polarized target, such as is currently available at HERMES.

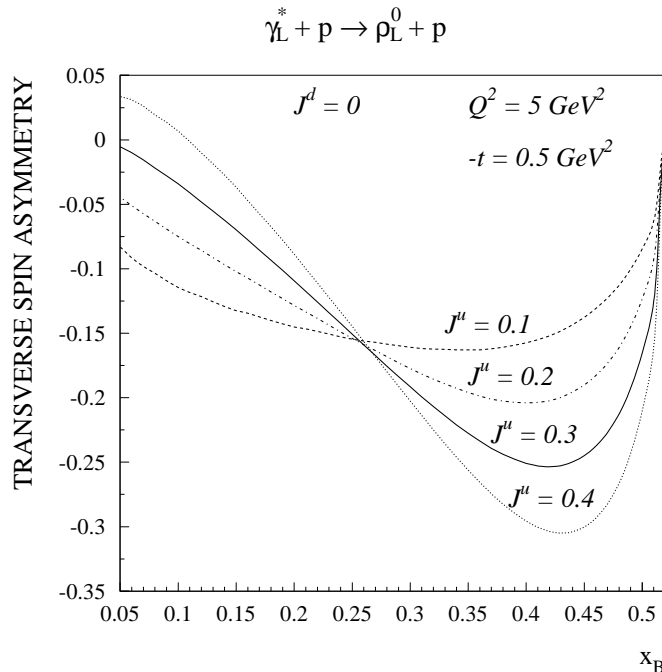


Figure 6. x_B dependence of the transverse spin asymmetry for the $\gamma_L^* p \rightarrow \rho_L^0 p$ reaction. The estimates are given using the model for the GPDs E^u and E^d as described in Ref. [3]. The curves show the sensitivity to the value of J^u as indicated on the curves (for a value $J^d = 0$).

In conclusion, we have seen some very promising first glimpses of GPDs entering hard exclusive reactions at the existing facilities. A dedicated program aiming at the extraction of the full physics potential contained in the GPDs will also require a dedicated facility combining high luminosity and a good resolution (in order to fully resolve the exclusive final state), as discussed at this Workshop, see [33–35].

REFERENCES

1. X. Ji, *J. Phys. G* **24**, 1181 (1998).
2. A.V. Radyushkin, in the Boris Ioffe Festschrift 'At the Frontier of Particle Physics / Handbook of QCD', edited by M. Shifman (World Scientific, Singapore, 2001).
3. K. Goeke, M.V. Polyakov, M. Vanderhaeghen, *Prog. Part. Nucl. Phys.* **47**, 401 (2001).
4. D. Müller, D. Robaschik, B. Geyer, F.-M. Dittes, and J. Horejsi, *Fortschr. Phys.* **42**, 101 (1994).
5. A.V. Radyushkin, *Phys. Rev. D* **59**, 014030 (1999); *Phys. Lett. B* **449**, 81 (1999).
6. M.V. Polyakov, and C. Weiss, *Phys. Rev. D* **60**, 114017 (1999).
7. M. Burkardt, *Phys. Rev. D* **62**, 071503 (R) (2000); M. Burkardt, hep-ph/0207047.
8. M. Diehl, hep-ph/0205208.
9. A.D. Martin, R.G. Roberts, W.J. Stirling, R.S. Thorne, *Phys. Lett. B* **531**, 216 (2002).
10. M.K. Jones *et al.*, *Phys. Rev. Lett.* **84**, 1398 (2000).
11. O. Gayou *et al.*, *Phys. Rev. Lett.* **88**, 092301 (2002).
12. M. Guidal, M.V. Polyakov, and M. Vanderhaeghen, forthcoming.
13. A.V. Radyushkin, *Phys. Rev. D* **58**, 114008 (1998).
14. M. Diehl, T. Feldmann, R. Jakob, and P. Kroll, *Eur. Phys. J. C* **8**, 409 (1999).
15. P. Kroll, M. Schürmann and P.A.M. Guichon, *Nucl. Phys.* **A598**, 435 (1996).
16. M. Vanderhaeghen, P.A.M. Guichon, and M. Guidal, *Phys. Rev. Lett.* **80**, 5064 (1998).
17. P.A.M. Guichon and M. Vanderhaeghen, *Prog. Part. Nucl. Phys.* **41**, 125 (1998).
18. A. Airapetian *et al.* (HERMES Collaboration), *Phys. Rev. Lett.* **87**, 182001 (2001).
19. S. Stepanyan *et al.* (CLAS Collaboration), *Phys. Rev. Lett.* **87**, 182002 (2001).
20. N. Kivel, M.V. Polyakov, and M. Vanderhaeghen, *Phys. Rev. D* **63**, 114014 (2001).
21. A.V. Belitsky, D. Müller, and A. Kirchner, *Nucl. Phys.* **B629**, 323 (2002).
22. L. Elouadrhiri, contribution to the proceedings.
23. B. Mecking, contribution to the proceedings.
24. D. Hasch, contribution to the proceedings.
25. K. Rith, contribution to the proceedings.
26. S.J. Brodsky, F.E. Close and J.F. Gunion, *Phys. Rev. D* **6**, 177 (1972).
27. V. Petrov *et al.*, *Phys. Rev. D* **57**, 4325 (1998).
28. F. Ellinghaus, contribution to the proceedings.
29. J.C. Collins, L.L. Frankfurt, and M. Strikman, *Phys. Rev. D* **56**, 2982 (1997).
30. L. Mankiewicz, G. Piller, and T. Weigl, *Eur. Phys. J. C* **5**, 119 (1998).
31. A. Airapetian, *et al.* (HERMES Collaboration), *Eur. Phys. J. C* **17**, 389 (2000).
32. M. Vanderhaeghen, P.A.M. Guichon, and M. Guidal, *Phys. Rev. D* **60**, 094017 (1999).
33. M. Guidal, contribution to the proceedings.
34. D. von Harrach, contribution to the proceedings.
35. R. Milner, contribution to the proceedings.